Journal of Hydro-environment Research 56 (2024) 17–27

Contents lists available at ScienceDirect

Journal of Hydro-environment Research

journal homepage: www.elsevier.com/locate/jher

Enhancing non-newtonian fluid modeling: A novel extension of the cross flow curve model

Keivan Kaveh [*,1], Andreas Malcherek [2]

Institute of Water Engineering, Department of Hydromechanics and Hydraulic Engineering, Universität der Bundeswehr München, Werner-Heisenberg-Weg 39, Neubiberg 85577, Bavaria, Germany

ARTICLE INFO

Keywords:
Cohesive sediment suspension
Rheology
Flow curve
Flocculation

ABSTRACT

A number of viscosity and flow curve models can be used to numerically investigate the non-Newtonian behavior of fluids. Although particle size, grain size distribution and concentration play a crucial role in determining the viscosity and flow behavior of suspensions and colloidal systems, they are either ignored or considered indirectly in almost all models. We present a mathematical extension of the widely used Cross flow curve model to account for the effect of concentration and particle size in modeling viscosity and flow curves. In particular, this study takes into account a variable total number of individual particles in unit volume, which is assumed to be constant in other models. The proposed extension allows the flow curve to model suspensions that are typically shear-thinning but can also be Newtonian, or shear-thickening for at different shear rates and concentrations. These considerations provide insight into studying and designing suspensions, colloidal systems, and other complex fluid–solid interactions.

1. Introduction

Rheology is the scientific study of how matter deforms and flows. The rheology of suspensions of cohesive sediments, also known as mud or slurry, is a complex and specialized area of study within the broader field of rheology. It involves the study of the flow and mechanical properties of sediment–water mixtures that contain cohesive, fine particles. These sediments often exhibit unique and challenging rheological behavior due to the cohesive forces between the particles.

Understanding the rheological behavior of cohesive sediment suspensions, such as clay suspensions, is of great importance in a wide range of fields and industries. Examples include hydraulic engineering, where insights into dredging, hyperconcentrated flow, and erosion resistance are critical (e.g. Engelund and Zhaohui, 1984; Gularte et al., 1979); civil engineering, where this knowledge is used in the context of cement and grouts (e.g. Lapasin et al., 1983); and chemical engineering, where applications extend to understanding the rheology of ceramic materials (e.g. Moore, 1959). This interdisciplinary understanding of rheology contributes significantly to progress and efficiency in these diverse fields.

Rheological behaviour can be divided into Newtonian and non-Newtonian categories. Non-Newtonian fluids exhibit flow behavior that deviates from the simple linear relationship between shear stress and shear rate observed in Newtonian fluids. These fluids can be classified into several categories based on their rheological properties. Some common classifications includes Pseudoplastic (shear-thinning), dilatant (shear-thickening), Bingham plastic, and viscoplastic behaviour, which are characterized by unique viscosity responses to changes in shear stress or shear rate. These classifications provide a framework for understanding the diverse behaviors exhibited by non-Newtonian fluids, and they are crucial for designing and optimizing processes in various fields.

In rheological modeling, there are two distinct model ideas for using the yield point, which is the minimum stress or force that must be applied to a material before it begins to deform. The first variant requires a definition of the tensor of internal stresses in such a way that elastic components can be taken into account. The second variant assumes that the material behaves as a high viscosity fluid below the yield point. The most well-known example of this type is Cross (1965) or Carreau (1972) model, which are available in different versions.

According to Cross (1965), the largest and most important class of non-Newtonian fluids are those which exhibit pseudoplastic flow, i.e.,

* Corresponding author.
E-mail addresses: keivan.kaveh@unibw.de (K. Kaveh), andreas.malcherek@unibw.de (A. Malcherek).
[1] First author.
[2] Second author.

https://doi.org/10.1016/j.jher.2024.08.001
Received 23 November 2023; Received in revised form 29 July 2024; Accepted 13 August 2024
Available online 18 August 2024

which show a decrease in viscosity with increasing rate of shear. On the assumption that pseudoplastic flow is associated with the formation and rupture structural linkages, Cross (1965) derived a new flow equation which is probably the most widely used model. While this rheological model has its merits in capturing the complex behavior of non-Newtonian fluids, it also comes with certain disadvantages and limitations. First, the model ignores the dependence of viscosity on solid concentration. While some researchers have addressed this by incorporating concentration dependent boundary viscosities, this adjustment is not inherent in the Cross model. On the other hand, the effect of particle size and its distribution on the rheological behavior of suspensions is not considered and is still lacking in the literature. Therefore, more work is needed to develop models that accurately account for a wide range of particle sizes and suspension concentrations simultaneously.

The effect of suspension concentration on the rheological behavior of a suspension is a critical aspect of understanding how such systems behave. As the concentration of solid particles rises, the viscosity of the suspension generally increases. This is because there are more particles interacting with each other and the surrounding fluid, leading to higher resistance to flow. This increase in viscosity can sometimes be non-linear, particularly at high concentrations. At higher concentrations, the suspension may transition from a Newtonian behavior to shear-thinning or shear-thickening, depending on factors like particle size, shape, and surface properties. At high concentrations, the increased likelihood of particle–particle interactions can also lead to aggregation, which impacts the rheological behavior. Additionally, gravitational sedimentation may become more pronounced, affecting the flow behavior over time. Normally, The dependence of the viscosity of a solution on the concentration c (expressed as volume fraction or as, weight by volume) can be represented as a power series of the type

$$\mu = \mu_0\left(1 + a_1 c + a_2 c^2 + a_3 c^3 + \ldots\right) \tag{1}$$

where μ_0 is the viscosity of the pure solvent (Simha, 1949). Considerable experimental and theoretical effort has been devoted to a determination of the coefficient a_1, the so-called intrinsic viscosity, for suspensions of particles of various shapes since Einstein's (Einstein, 1905) original hydrodynamic treatment of spheres.

Particle size is one of the most important characteristics of particulate materials. As shown in Fig. 1, smaller particle size for a given solid fraction results in an increase in the number of particles in a given volume. As a result, the smaller particles have a significantly larger particle surface area. The dynamics of very small particles involves Brownian motion against an applied shear force, as observed by Perrin (1910), electrostatic repulsion, or steric hindrance.

At elevated shear rates, the viscosity contrast between small and large particles diminishes due to favorable rearrangement along the flow direction, as illustrated in Fig. 2.

Monodisperse materials consist of particles or molecules that are

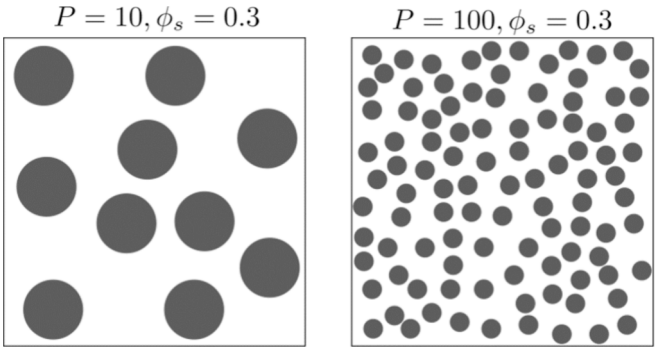

Fig. 1. Constant solid fraction $\phi_s = 0.3$ with different sphere size, P is number of particles (modified from Anton Paar GmbH Sitemap).

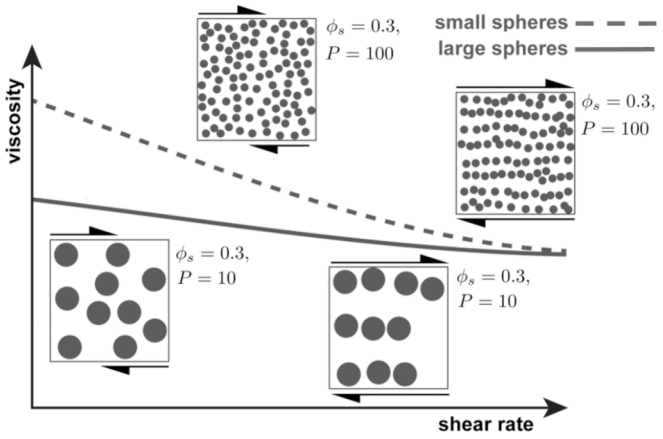

Fig. 2. The variation in shear rate for both small and large spheres for a constant solid fraction (modified from Anton Paar GmbH Sitemap).

nearly the same size and shape. In other words, the size distribution is very narrow, and all particles are uniform. However, in most suspensions, the particle sizes are not uniform. The optimal packing density, and therefore the maximum solid fraction, is enhanced by having particles of different sizes (polydispersity). This variability allows for more efficient space filling. A wider particle size distribution has a more pronounced positive effect on packing density. Uniform materials tend to have lower viscosities compared to non-uniform materials with the same volume fraction. This is because the uniformity in particle size reduces the friction and collisions between particles, making the material flow more smoothly.

Comparing the viscosity of two monodisperse suspensions with a polydisperse, Fig. 3 shows a bigger viscosity for the polydisperse mixture. However, it is worth noting that if the material size is greatly reduced, then smaller particles will tend to increase the viscosity for a given shear rate and solids content (Ancey and Jorrot, 2001). In colloidal suspensions with bimodal particle size distributions, smaller particles can act as lubricants (Ancey, 2001).

2. Theory description

In the following sections, we propose two different hypotheses for analyzing and understanding the rheological behavior of the suspensions at hand. These hypotheses represent different conceptual frameworks and assumptions, each offering a unique perspective on the matter under investigation. The application of these two hypotheses serves to explore the problem comprehensively, shedding light on its intricacies from multiple angles. By considering these different

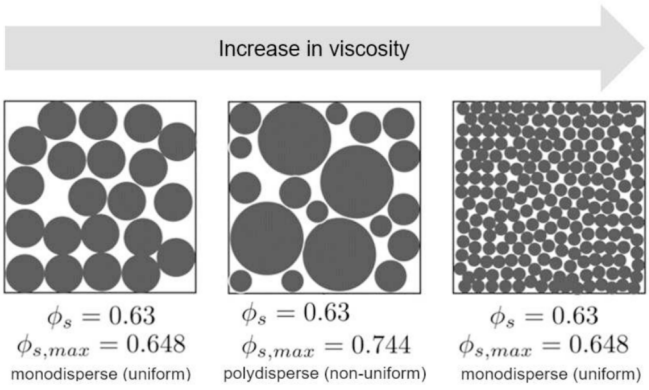

Fig. 3. Effect of particle size and polydispersity on viscosity: Comparison of small and large spheres under constant solid fraction and shear rate.

viewpoints, we aim to provide a well-rounded and nuanced understanding of the issue, allowing for different potential explanations and interpretations that may enrich our overall understanding.

2.1. The first hypothesis

Under the premise that particles form linear chains resembling rigid rods, Casson (1959) formulated a theory tailored for nonaqueous pigment suspensions. However, challenging this assumption, Cross (1965) embraced a more straightforward approach. This alternative method considers a random chain formation, yielding a novel form of the flow equation. In fact, he postulates that flocculation involves the presence of interconnected particle groups. Under conditions of steady shear, there is an average group size that depends on the intensity of the applied shear. These groups are assumed to have the structure of randomly kinked chains. Finally, the equilibrium of an average chain having L linkages is considered as

$$\frac{dL}{dt} = k_2 P - \left(k_0 + k_1 \dot{\gamma}^n\right) L \tag{2}$$

where $\dot{\gamma}$ is applied shear rate in reciprocal seconds; P is total number of single particles (linked or otherwise) in unit volume; $k_0 + k_1\dot{\gamma}^n$ is assumed to be the effective rate constant for rupture, i.e. breakdown involves the nth power of the shear rate; and k_2 is a constant.

To gain further insight into the non-Newtonian rheology of suspensions, it is useful to consider particle properties for a comprehensive characterization of suspensions. Here we assume that when a bond is formed between particles in a suspension and they stick together, they form a new, single, larger particle. This changes the overall rheological behavior of the system and is often associated with the idea of flocculation, the process of particles coming together to form larger aggregates or flocs.

A link between the total number of particles per unit of volume at time t and the number of primary particles $N(t)$ inside a floc of size $d_f(t)$ is defined by Ali and Chassagne (2022) as

$$P\left(t\right) = \frac{\phi_s}{N\left(t\right) d_p^3} \tag{3}$$

where ϕ_s is volume fraction of primary particles in suspension and d_p is particle size.

According to Kranenburg (1994), the relation between number of primary particles in a floc and floc size is given as

$$N\left(t\right) = \left(\frac{d_f\left(t\right)}{d_p}\right)^{n_f} \tag{4}$$

where n_f is usually termed "fractal dimension", in reference to the study of the flocculation of monodisperse primary particles.

Substituting Eq. (4) into Eq. (3) gives

$$P\left(t\right) = \phi_s \frac{d_f^{-n_f}}{d_p^{3-n_f}} \tag{5}$$

We have here made the assumption that only one sediment fraction is present. From Eq. (5) it follows that when $n_f < 3$ the number of individual particles P decreases with increasing sediment size d_p. In Winterwerp (1998), the fractal dimension of the mud flocs is assumed to be 2 (although n_f is known to range between 1.8 and 2.5). A more legitimate consideration is suggested by Khelifa and Hill (2006), which considers a continuous decrease in the fractal dimension as the size of the flocs increases. In this context, however, we consider the constant fractal dimension n_f for the sake of simplicity. From Eq. (5) it is also clear that the total number of single particles increases as the sediment fraction ϕ_s increases.

Combining Eq. (2) and Eq. (5) gives

$$\frac{dL}{dt} = k_2 \phi_s \frac{d_f^{-n_f}}{d_p^{3-n_f}} - \left(k_0 + k_1 \dot{\gamma}^n\right) L \tag{6}$$

Two concepts, the equilibrium flow curve and the steady shear flow curve, are often associated with the study of rheology. Here we use the concept of the equilibrium flow curve, which describes the behavior of the material under constant stress and allows the system to reach a stable, long-term state. Equilibrium is attained when $dL/dt = 0$, hence

$$L = k_2 \phi_s \frac{d_{f,eq}^{-n_f}}{d_p^{3-n_f}} \frac{1}{k_0 + k_1 \dot{\gamma}^n} \tag{7}$$

where $d_{f,eq}$ is the equilibrium floc size.

Considering $L = L_0$ when $\dot{\gamma} = 0$, we obtain

$$L_0 = \frac{k_2 \phi_s}{k_0} \frac{d_{f,0}^{-n_f}}{d_p^{3-n_f}} \tag{8}$$

where $d_{f,0}$ is the initial floc size when $\dot{\gamma} = 0$.

Dividing Eq. (7) by Eq. (8), one can obtain L/L_0 as

$$\frac{L}{L_0} = \left(\frac{d_{f,0}}{d_{f,eq}}\right)^{n_f} \frac{1}{1 + \beta \dot{\gamma}^n} \tag{9}$$

where $\beta = k_1/k_0$. It is now necessary to relate L/L_0 to viscosity of system. Similar to Cross (1965), it can be obtained as

$$\frac{L}{L_0} = \frac{\mu - \mu_\infty}{\mu_0 - \mu_\infty} \tag{10}$$

where μ_0 and μ_∞ are viscosity when $\dot{\gamma} = 0$ and $\dot{\gamma} \to \infty$, respectively.

Combining Eqs. (9) and (10) gives the new proposed flow equation as

$$\mu = \mu_\infty + \left(\frac{d_{f,0}}{d_{f,eq}}\right)^{n_f} \frac{\mu_0 - \mu_\infty}{1 + \beta \dot{\gamma}^n} \tag{11}$$

where $\left(d_{f,0}/d_{f,eq}\right)^{n_f}$ is the extension factor that relates the viscosity to the equilibrium floc size. It should be noted that Eq. (11) refers to equilibrium value of viscosity.

In our rheological model, we take into careful consideration the impact of both concentration and sediment size, recognizing that these factors play pivotal roles in shaping the model's outcomes. The equilibrium floc size, which is a fundamental determinant of a suspension's rheological behavior, is intricately tied to these parameters. Concentration affects the extent of particle–particle interactions and the overall density of the suspension, which, in turn, influences floc formation and size. Moreover, sediment size directly influences the agglomeration tendencies and the ease with which particles can form stable flocs. By incorporating these crucial parameters into our rheological model, we ensure a more accurate representation of the real-world behavior of suspensions, allowing us to make informed predictions and optimize processes across a range of applications where such systems are encountered.

2.2. The second hypothesis

The second hypothesis assumes that there is a direct relationship between floc size and the number of linkages between particles. That is, as the number of links between particles increases, we expect the floc size to increase proportionally. In other words, we believe that the two variables are positively correlated and that changes in one will result in corresponding changes in the other ($L \propto d_f$).

The relationship between floc size and the number of linkages between particles in a colloidal system can be complex and may depend on various factors such as the nature of the particles, the type and concentration of the dispersing medium, and the presence of additives. However, a simplified equation to represent a hypothetical relationship

might be expressed as:

$$d_f = kL^m \tag{12}$$

where k is a constant representing the strength of each linkage and m is an exponent that characterizes the nature of the relationship. This equation suggests that the floc size is related to the number of linkages, with the strength of the linkages represented by the constant k, and the exponent m determining how the floc size changes concerning the number of linkages.

It is important to note that the actual relationship between floc size and the number of linkages is likely to be more complex and may involve additional factors. Experimental data and a more detailed understanding of the specific colloidal system would be needed to develop a more accurate and applicable equation.

Using Eq. (12), the rate of change of the number of links can be expressed as

$$\frac{dL}{dt} = \frac{1}{mk^{1/m}} d_f^{1/m-1}\left(\frac{dd_f}{dt}\right) \tag{13}$$

The equilibrium is reached when $dL/dt = 0$, which corresponds to $dd_f/dt = 0$. Consequently, $dd_f/dt = 0$ leads to $d_{f,eq}$. Essentially, in the state of equilibrium, L can be linked to the equilibrium flock size, and this relationship is represented by substituting $d_{f,eq}$ for d_f in Eq. (12) as

$$L = \left(\frac{d_{f,eq}}{k}\right)^{1/m} \tag{14}$$

Similarly, considering $L = L_0$ when $\dot{\gamma} = 0$, we need to substitute $d_{f,0}$ for d_f in Eq. (12), which gives

$$L_0 = \left(\frac{d_{f,0}}{k}\right)^{1/m} \tag{15}$$

Applying Eqs. (14) and (15), one can obtain L/L_0 as

$$\frac{L}{L_0} = \left(\frac{d_{f,eq}}{d_{f,0}}\right)^{1/m} \tag{16}$$

For the sake of simplicity in our analysis, we make the assumption that the floc size at zero shear rate is equal to the primary particle size, that is $d_{f,0} = d_p$. The assumption that no aggregation or breakup occurs at zero shear rate can be reasonable in certain contexts, depending on the specific characteristics of the system being studied. However, it is important to consider the nature of the material and the conditions under which it is being modeled.

This assumption allows us to establish a baseline reference point where there is minimal or no shear-induced deformation of the particles within the colloidal system. While real-world conditions may lead to some variations, this assumption simplifies our calculations and provides a useful starting point for understanding the impact of shear rate on floc size. It is important to acknowledge that this assumption serves as a simplification and may not hold under all circumstances, but it aids in making our analysis more manageable and serves as a valuable initial approximation. With this assumption Eq. (17) can be expressed as

$$\frac{L}{L_0} = \left(\frac{d_{f,eq}}{d_p}\right)^{1/m} = \left(\widehat{d}_{f,eq}\right)^{1/m} \tag{17}$$

where $\widehat{d}_{f,eq}$ is the dimensionless equilibrium floc size.

In order to obtain the right values at boundaries when $\dot{\gamma}\to 0$ and ∞, it is now necessary to relate L/L_0 to μ/μ_m which results in

$$\mu = \left(\frac{d_{f,eq}}{d_p}\right)^{1/m} \mu_m = \left(\widehat{d}_{f,eq}\right)^{1/m} \mu_m \tag{18}$$

where $\left(d_{f,eq}/d_p\right)^{1/m} = \left(\widehat{d}_{f,eq}\right)^{1/m}$ is the extension factor for the second model.

2.3. Derivation of the extension factors and final models

In order to define the extension factors in detail, examining the equilibrium solution of floc size is required. For this purpose, we describe the governing equations for floc size through an equilibrium assumption to yield an equation for the equilibrium floc size based on aggregation and breakup rates. The extension factor is then again calculated using the obtained equations. With this approach, there is a built in assumption that flocs are in equilibrium with the local conditions since time dependence is removed.

Using the relationship between the sediment mass concentration c, the aggregate structure of a floc (assumed to be a 3-D fractal entity), the shear-driven collision kinetics, and a proposed floc erosion or break-up rate model based on turbulent shear, Winterwerp (1998) showed that the conservation equation can be written as a rate equation for the average floc size as follows

$$\frac{dd_f}{dt} = \underbrace{\frac{k_A'}{n_f}\frac{c}{\rho_s} d_p^{n_f-3} d_f^{4-n_f}\dot{\gamma}}_{Aggregation} \underbrace{-\frac{k_B'}{n_f} d_f\dot{\gamma}\left(\frac{d_f - d_p}{d_p}\right)^p \left(\frac{\tau_t}{\tau_y}\right)^q}_{Breakup} \tag{19}$$

where $\tau_t = \mu\dot{\gamma}$ is the turbulence-induced stress on the floc, and $\tau_y = F_y/d_f^2$ represents the strength of the floc, where F_y is the floc yield strength in dimension of force. Two dimensionless primary model coefficients, k_A' and k_B', are the aggregation and breakup coefficients, respectively which play a key role in this context. The aggregation coefficient is influenced by the efficiency of statistical collisions leading to aggregation and a floc shape factor. Both k_A' and k_B' are calibration parameters and are determined by factors such as sediment adhesion properties, which are influenced by primary particle size, sediment mineralogy, water chemistry, organic matter, and particle shape (Kuprenas et al., 2018). In addition, the nondimensional power coefficients in the floc erosion rate kernel must be determined. These are denoted as p and q.

The equilibrium value of the floc size $d_{f,eq}$ can be calculated if dd_f/dt in Eq. (19) is set to zero, i.e., the aggregation and breakup rates are balanced. Letting $dd_f/dt = 0$ and assuming that $d_{f,eq} \gg d_p$, the equilibrium floc size can be obtained as

$$d_{f,eq} = \left[\alpha' c\dot{\gamma}^{-q}\right]^{1/\left(2q+p+n_f-3\right)} \tag{20}$$

where

$$\alpha' = \frac{1}{\rho_s}\frac{k_A'}{k_B'} d_p^{n_f+p-3}\left(\frac{\mu}{F_y}\right)^{-q} \tag{21}$$

Numerous studies have established a proportional relationship between the equilibrium floc size and the Kolmogorov microscale. In particular, it has been found that $d_{f,eq}\propto\dot{\gamma}^{-1/2}$, as shown in studies by Eisma (1986), Scully and Friedrichs (2007), Verney et al. (2009). To maintain this proportionality, Winterwerp (1998) emphasized that the exponent p should satisfy the condition that it is equal to $3-n_f$, or equivalently, that $p+nf-3=0$ (Kuprenas et al., 2018). Thus, Eqs. (20) and (21) reduce to

$$d_{f,eq} = (\alpha' c)^{1/2q}\dot{\gamma}^{-1/2} \tag{22}$$

and

$$\alpha' = \frac{1}{\rho_s}\frac{k_A'}{k_B'}\left(\frac{\mu}{F_y}\right)^{-q} \tag{23}$$

To ensure that Eq. (22) is valid when $\dot{\gamma} = 0$ and $d_{f,eq} \neq 0$ when $\dot{\gamma}\to\infty$ or $\phi_s\to 0$, it is modified here as

$$d_{f,eq} = (\alpha' c)^{\frac{1}{2q}}\frac{1}{\left(k_0' + k_1'\dot{\gamma}^{1/2}\right)} + d_p \tag{24}$$

where k_0' and k_1' are constants. Setting $\dot{\gamma} = 0$ in Eq. (24), we obtain $d_{f,0}$ as

$$d_{f,0} = \frac{1}{k_0'}(\alpha' c)^{\frac{1}{2q}} + d_p \tag{25}$$

Finally, the proposed extension factor can be obtained by dividing Eq. (25) by Eq. (24) and exponentiating to the power of n_f as

$$F\left(c, \dot{\gamma}\right) = \left(\frac{d_{f,0}}{d_{f,eq}}\right)^{n_f} = \left[\frac{1 + A(\alpha' c)^{1/2q}}{1 + B(\alpha' c)^{1/2q}}\right]^{n_f} \tag{26}$$

where $A = 1/\left(d_p k_0'\right), B = 1/\left(d_p k_0'\left(1 + \beta' \dot{\gamma}^{1/2}\right)\right)$ and $\beta' = k_1'/k_0'$. To determine the behavior of the function F, i.e. Eq. (26), as shear rate approaches zero and infinity, one can look at the limits of the function as

$$\lim_{\dot{\gamma}\to\infty} F\left(c, \dot{\gamma}\right) = \left(1 + A(\alpha' c)^{1/2q}\right)^{n_f} \tag{27}$$

$$\lim_{\dot{\gamma}\to 0} F\left(c, \dot{\gamma}\right) = 1 \tag{28}$$

So there is a transition function that helps to achieve smooth and continuous changes between these two states or conditions. Understanding this transition function is fundamental to mathematical modeling. This allows us to describe and analyze the proposed model, providing a mathematical representation of how one variable changes with respect to another.

Here we define the dimensionless equilibrium floc size as

$$\widehat{d}_{f,eq} = \frac{d_{f,eq}}{d_p} = 1 + B(\alpha' c)^{1/2q} \tag{29}$$

Therefore, Eq. (26) can also be rewritten as

$$F\left(c, \dot{\gamma}\right) = \left[\frac{1 + A(\alpha' c)^{1/2q}}{\widehat{d}_{f,eq}}\right]^{n_f} \tag{30}$$

As can be seen from Eq. (30), the transition from the lower bound to the upper bound is made by the dimensionless floc size.

Finally, substituting Eq. (30) into Eq. (11) gives

$$\mu = \mu_\infty + \left[\frac{1 + A(\alpha' c)^{1/2q}}{\widehat{d}_{f,eq}}\right]^{n_f} \frac{\mu_0 - \mu_\infty}{1 + \beta \dot{\gamma}^n} \tag{31}$$

Note that if β' is chosen to be large, then $B \to 0$ and therefore Eq. (31) is reduced to

$$\mu = \mu_\infty + \left[1 + A(\alpha' c)^{1/2q}\right]^{n_f} \frac{\mu_0 - \mu_\infty}{1 + \beta \dot{\gamma}^n} \tag{32}$$

Eq. (31) is the final form of the model proposed based on the first hypothesis. A notable feature of Eq. (31) is its ability to yield different initial viscosities at zero shear rate for the same sample at different concentrations. This is in contrast to the original Cross model, which requires the specification of a single μ_0 value for each flow curve, regardless of whether they are from the same sample but at different concentrations. Eq. (31) shows that viscosity remains dependent on both concentration and grain size even as the shear rate approaches zero.

Similarly, substituting Eq. (29) into Eq. (18) gives the final form of the proposed model based on the second hypothesis as

$$\mu = \left[1 + B(\alpha' c)^{1/2q}\right]^{1/m} \mu_m \tag{33}$$

It is imperative to recognize that Eq. (33) eliminates the need to specify upper and lower viscosity limits, which is a notable advantage, especially in terms of computational simplicity and straightforward applicability. Moreover, the formulation obviates the need to define the parameters n and β, which are required in the context of the first hypothesis. This feature makes the second hypothesis much more straightforward, offering improved simplicity while taking into account the influence of particle size and concentration.

3. Experimental data

Two samples were collected from the Ems estuary at Gandersum and Jemgum for characterization purposes. The assessment involved the determination of the loss on ignition, serving as an indicator of the organic content of the samples, and the grain size distribution, which was measured through triple analyses. The Gandersum (G) sample exhibited a loss on ignition of 8.9 %, while the Jemgum (J) sample recorded 5.6 %. The particle size distribution is illustrated in Fig. 4, showcasing similar grading curves, and the median grain diameters are denoted as $d_G = 15.2$ µm and $d_J = 17.4$ µm. The solid content of the samples was ascertained by subjecting them to a 24-h drying process in a drying oven at 105 °C. The sediment density was determined to be 2650 kg/m^3 and the water density was established as 1000 kg/m^3. The samples in their original state had a solids content of $\phi_s = 0.2$. The solid fractions $\phi_s = 0.16$, 0.13, 0.10 and 0.07 were then produced.

Depending on the site and the sampling point, the samples are given the corresponding designation $G_{0.16}$, $G_{0.13}$, and so on. Fig. 5 clearly shows that the samples with a solids content of $\phi_s = 0.16$ tend to have a solid character, and those with $\phi_s = 0.07$ tend to have a liquid character.

Rotation tests were performed with a rheometer (Physica MCR301 from Anton Paar GmbH), a plate measuring system with a diameter of 60 mm (PP60/Ti-SN1493) and a gap distance of 1 mm. Rotation tests were performed in controlled shear stress (CSS) mode for 20 s at a shear rate of $\dot{\gamma} = 5$ s^{-1} shear rate. This was followed by a rest period of 30 s. The measurements were then performed in the shear stress range given in Table 1, starting with 5 s measurement point duration and decreasing logarithmically to 1 s measurement point duration. In total, a maximum of 140 test points were excluded or the test was terminated when a maximum shear rate of 100 s^{-1} was reached. This corresponds to the measurement protocol presented by Chmiel et al. (2020).

The third sample (*M*) was also collected from the Ems estuary. The measurement technique used for this sample differs from that used for the other two samples. As a result, it shows a distinct behavior that distinguishes it from the other two and is therefore selected for model evaluation here. The solid content of the sample was ascertained by subjecting it to a 24-h drying process in a drying oven at 105 °C and exhibited a loss on ignition of 10.5 % The samples in their original state had a solids content of $\phi_s = 0.1$. The solid fractions $\phi_s = 0.085$, 0.07 and 0.055 were then produced. Then, the dynamic viscosity and shear rate of the sample was determined over 50 measuring points with for each solid fraction. For this sample, rotation tests were performed with a rheometer (Physica MCR301 from Anton Paar GmbH), a plate measuring system with a diameter of 60 mm (PP60/Ti-SN1493) and a gap distance of 0.5 mm. Rotation tests were performed in controlled rating (CR) mode. Here a certain speed of the plate is set and the shear stress required for this is measured.

4. Result and discussion

4.1. Analysis of the first model

Fig. 6 illustrates the investigation of the extension factor, as defined by Eq. (30), in the context of a constant sediment fraction $\phi_s = 0.1$. The plotted results suggest that there is a visible and expected trend: as the rate of aggregation to breakup (α') increases, neighboring particles attract each other more and particles will cluster together to form flocs. As flocs are porous and behave as rigid particles when slowly sheared by the suspending fluid, flocculation increases the apparent viscosity of the suspension (Fusier et al., 2018). As can be seen from Fig. 6, at higher shear rates the extension factor becomes constant and viscosity decreases to its lower boundary value μ_∞.

Fig. 7 shows the variation of the extension factor and application of

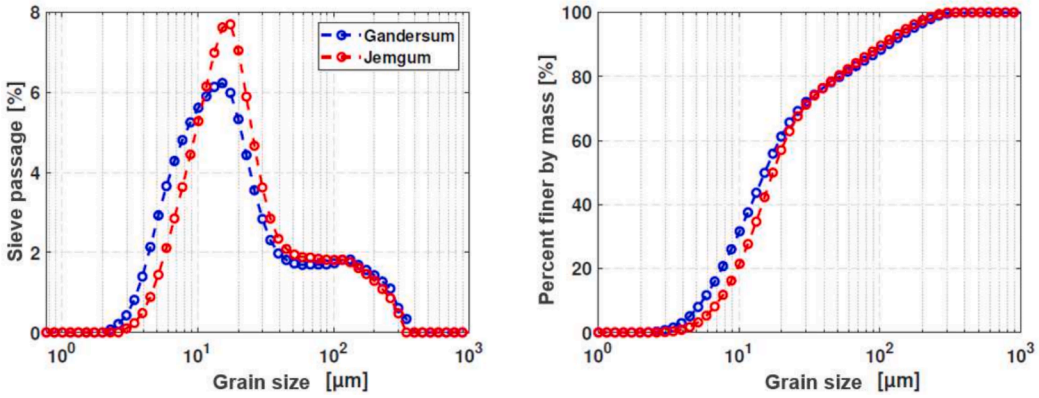

Fig. 4. Sieve curves and grain size distribution of the Gandersum (*G*) and Jemgum (*J*) silt samples.

Fig. 5. Gandersum (*G*) and Jemgum (*J*) silt samples with the volumetric solid fractions $\phi_s = 0.16$, 0.13, 0.10 and 0.07.

Table 1
Overview of the measurements carried out with default parameters.

Sample	Shear stress range measurement (CSS)
$G_{0.16}$	$\tau = 40$–600 Pa
$G_{0.13}$	$\tau = 20$–400 Pa
$G_{0.10}$	$\tau = 10$–200 Pa
$G_{0.07}$	$\tau = 0.1$–50 Pa
$J_{0.16}$	$\tau = 40$–600 Pa
$J_{0.13}$	$\tau = 20$–400 Pa
$J_{0.10}$	$\tau = 10$–200 Pa
$J_{0.07}$	$\tau = 0.1$–50 Pa

the new flow equation, represented by Eq. (31), with a constant sediment fraction $\phi_s = 0.1$ for different particle sizes. As expected, when particle size decreases, the total number of particles increases within the same volume concentration. Due to the increased number of smaller particles, there is a higher probability of particle collisions within the fluid, leading to the formation of larger aggregates or flocs. Similarly, at low shear rates, the disruptive forces are minimal and flocs create more structurally stable aggregates that resist deformation under shear. This resistance to flow results in an increase in viscosity for small shear rates. This is consistent with Fig. 2 and is a logical expectation since larger particles, with more mass and potentially less surface area, tend to exhibit less rapid or abrupt changes in viscosity in response to variations in shear rate.

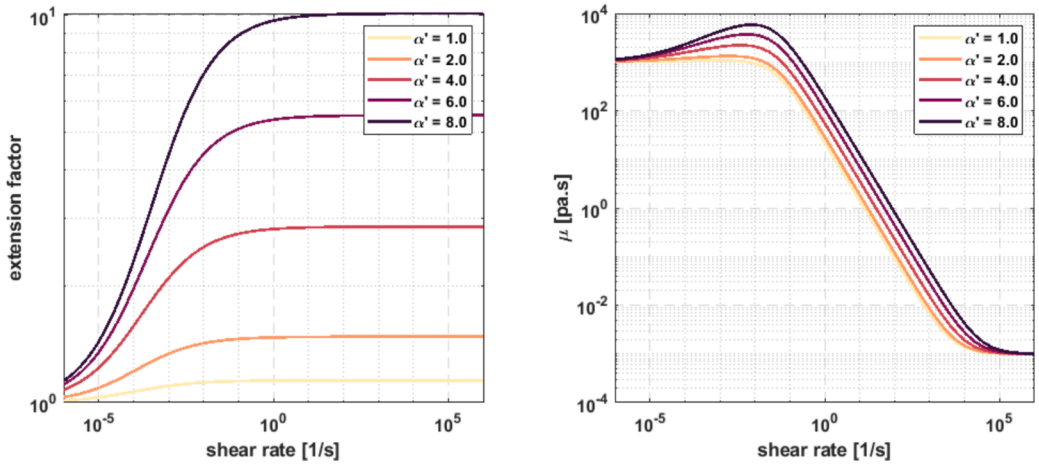

Fig. 6. Variation of (left) the extension factor, i.e. Eq. (30right) viscosity μ according to Eq. (31) with constant sediment fraction $\phi_s = 0.1$ for a range of α' values.

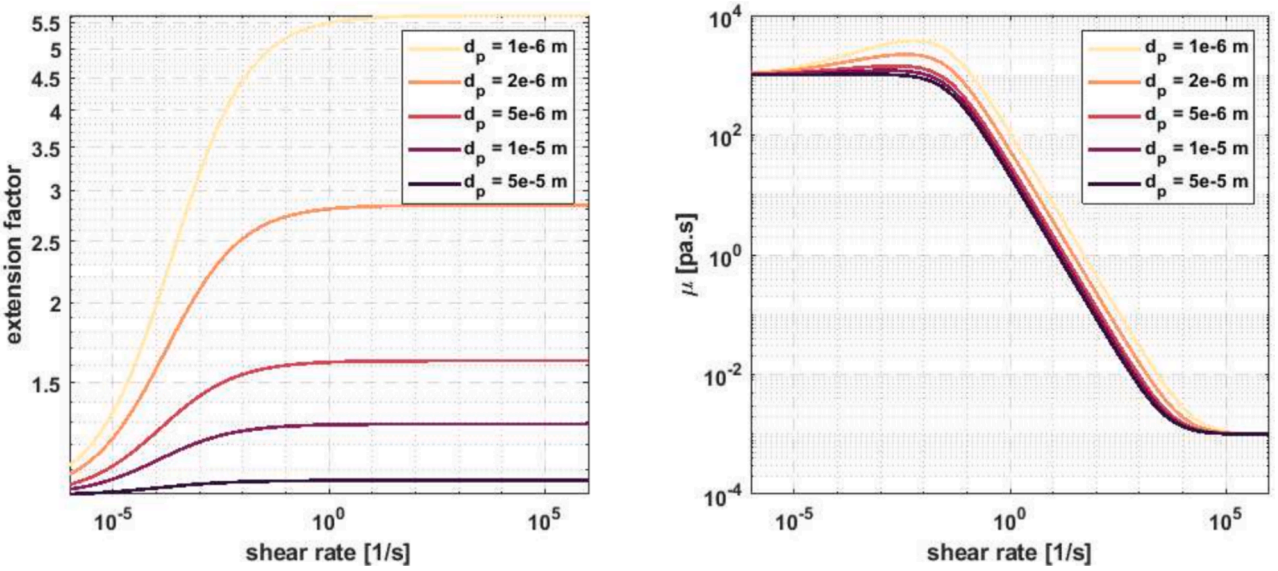

Fig. 7. Variation of (left) the extension factor, i.e. Eq. (30right) functionality of the new flow equation, i.e. Eq. (31), with constant sediment fraction $\phi_s = 0.1$ for a range of particle sizes d_p.

The relationship between viscosity and solid volume fraction in a suspension or colloidal system, which is not considered in the original Cross model, for different values of q and shear rates is depicted in Figs. 8 and 9, respectively. According to Fig. 8, as the value of parameter q increases, the variations in the extension factor $F(c, \dot{\gamma})$ with respect to the volumetric sediment fraction ϕ_s become less pronounced. Consequently, the variations in viscosity with sediment fraction also decrease.

For certain systems, especially those involving polymers or colloids, viscosity may continue to increase with concentration due to increased entanglements or interactions between polymer chains or particles. This behavior can be clearly seen in Fig. 9. It should also be noted that the rate of increase in viscosity with increasing solid volume fraction gets smaller at higher constant values of shear rate.

Fig. 10 shows a parametric plot of viscosity according to Eq. (31) as a function of two key variables: solid volume fraction ϕ_s on the x-axis, shear rate $\dot{\gamma}$ on the y-axis, with viscosity μ plotted on a logarithmic scale on the z-axis. As the solid volume fraction increases along the x-axis, the corresponding trend in viscosity becomes apparent. Specifically, the logarithmic scale on the z-axis shows that the viscosity exhibits a significant upward trend as the solid volume fraction increases. This behavior is consistent with the expected outcome in many complex fluid–solid systems, where an increase in the concentration of solid particles in a fluid medium typically leads to an increase in the resistance to flow, and hence an increase in viscosity. At the same time, the effect of shear rate, shown on the y-axis, becomes apparent. The logarithmic scale on the z-axis helps to visualize that as the shear rate increases, there is a noticeable decrease in viscosity.

4.2. Analysis of the second model

Model response to variation of volumetric sediment fraction ϕ_s and different values of constant shear rates $\dot{\gamma}$ according to Eq. (33) is shown in Fig. 11. The observed trends in this figure highlight the model's sensitivity to changes in sediment fraction, illustrating how alterations in the volume of sediment within the fluid affect the system's response. Furthermore, the diverse behavior under varying shear rates provides a comprehensive view of the model's dynamics across different flow conditions. The significance of shear rates in influencing the overall response of the system is evident. As expected at low shear rates, volumetric sediment concentration makes a noticeable difference in viscosity. As the shear rate is increased, the model viscosities approach the minimum predefined viscosity, which may be the viscosity of the fluid.

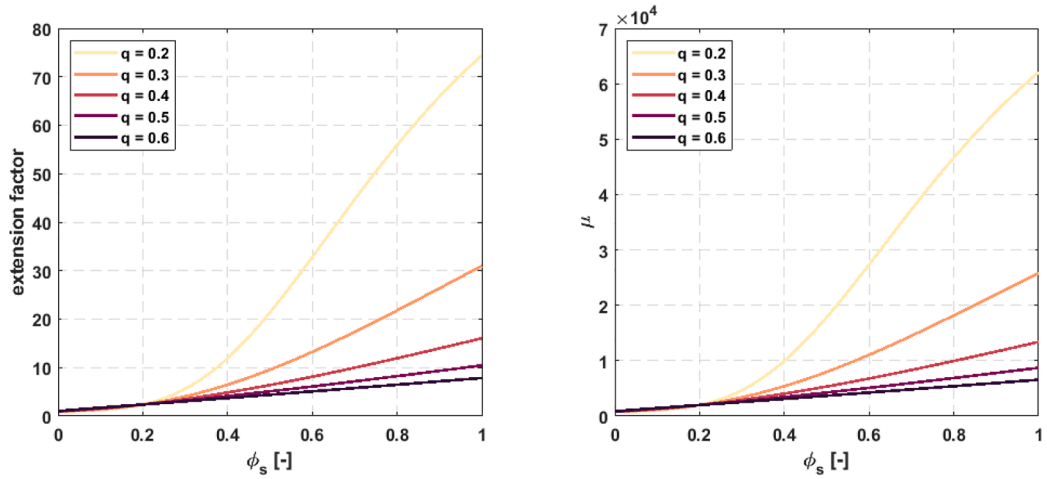

Fig. 8. Variation of (left) the extension factor, i.e. Eq. (30right) viscosity, i.e. Eq. (31), with constant shear rate $\dot{\gamma} = 0.01$ for a range of q.

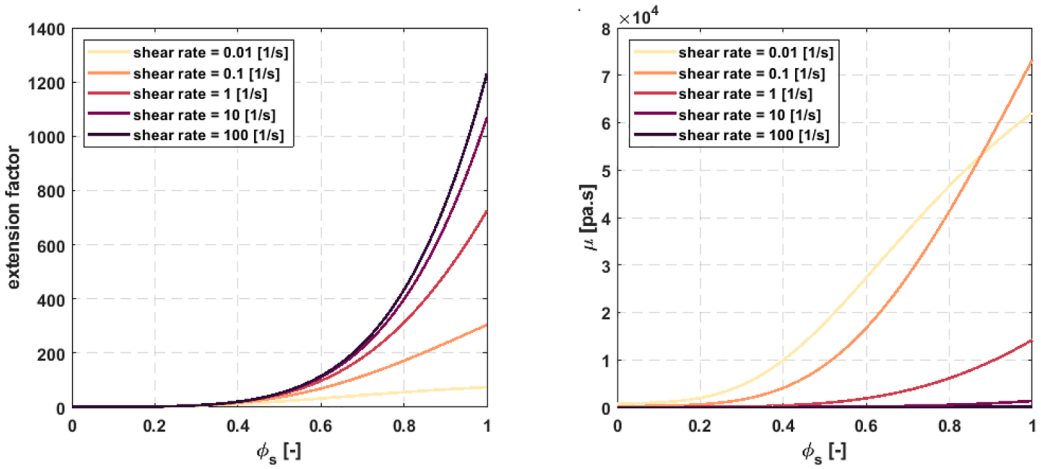

Fig. 9. Variation of (left) the extension factor, i.e. Eq. (30right) viscosity, i.e. Eq. (31), with constant q for different values of $\dot{\gamma}$.

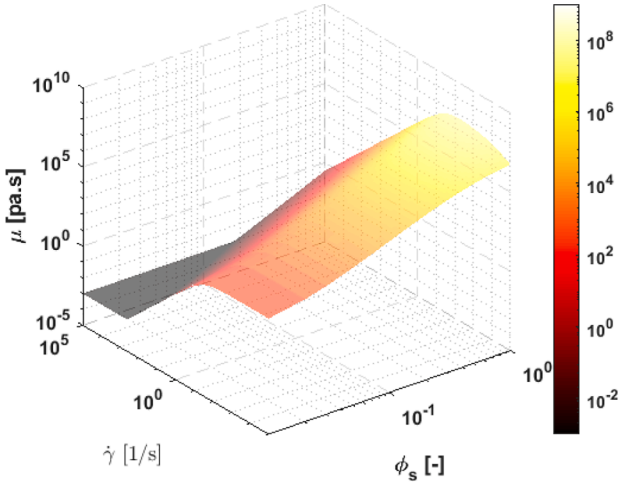

Fig. 10. Viscosity as a function of shear rate ($\dot{\gamma}$) and solid volume fraction (ϕ_s) according to Eq. (31).

This shows the transition from a sediment-influenced regime to a shear-dominated regime.

However, it should be noted that the absence of an increase in viscosity at low shear rates in the model is a consequence of neglecting the effect of floc formation. It is due to the assumptions made in this hypothesis and the consideration of $d_{f,0} = d_p$.

Fig. 12 illustrates a parametric plot of viscosity (Eq. (33)) with solid volume fraction ϕ_s on the x-axis and shear rate $\dot{\gamma}$ on the y-axis, with viscosity μ displayed on a logarithmic scale on the z-axis. As expected, an increase in solid volume fraction results in a substantial upward trend in viscosity, and an increase in shear rate correlates with a pronounced decrease in viscosity.

4.3. Model verification

Evaluation of the models with the tested samples $G_{0.16} - G_{0.07}$ and $J_{0.16} - J_{0.07}$ are shown in Figs. 13 and 14, where the measured values are represented by circles and the approximated models according to Eqs. (31) and (33) are represented by solid lines, respectively. The figures show the viscosities as a function of the shear rate. All samples show non-Newtonian, shear-thinning behavior, as the viscosities decrease with increasing shear stress. As can be seen from Figs. 13 and 14, there is an acceptable agreement between the measured data and the simulated results. The visual comparison between the experimental observations and the simulated results shows a close match, indicating that the simulation accurately captures the essential features of the system under study.

To account for the effect of solid volume fraction or concentration on viscosity, researchers typically consider variable boundary viscosities (i.e., μ_0 and μ_∞) for each concentration in the classical Cross model. This is usually accomplished by treating the boundary viscosities as an exponential function of the solid volume fraction or concentration. However,

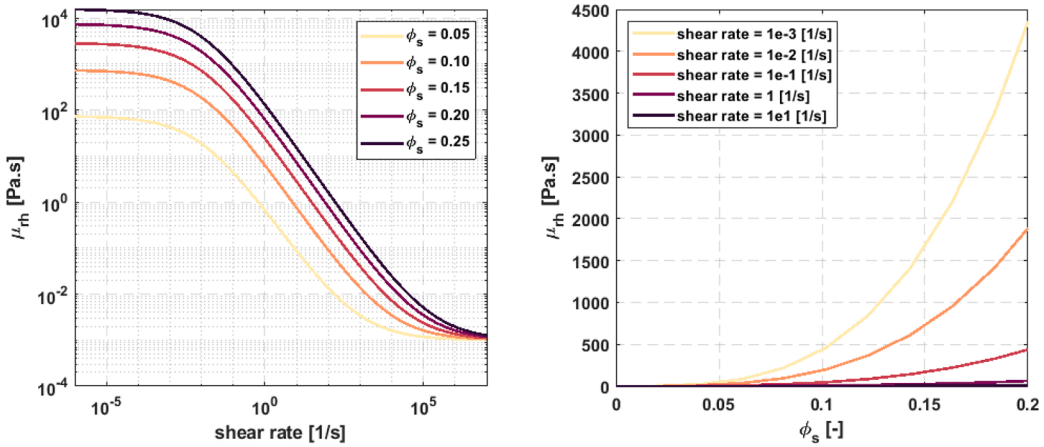

Fig. 11. Model response to (left) variation of volumetric sediment fraction (ϕ_s) and (right) different values of constant shear rates ($\dot{\gamma}$) according to Eq. (33).

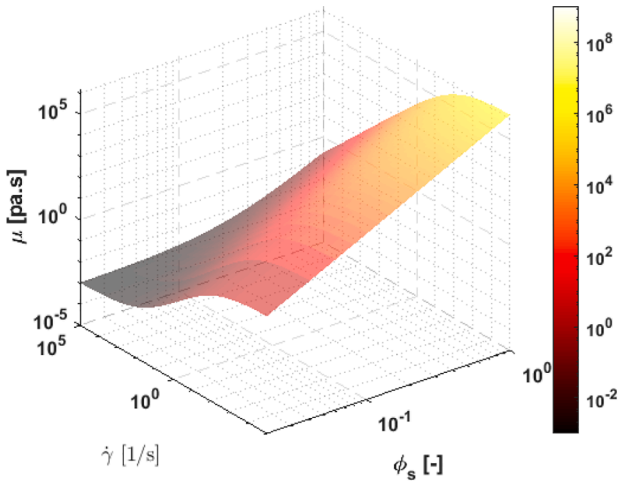

Fig. 12. Viscosity as a function of shear rate ($\dot{\gamma}$) and solid volume fraction (ϕ_s) according to Eq. (33).

in the present modeling framework, it is imperative to emphasize that all parameters, including the boundary viscosities described in Eq. (31), remain constant for each flow curve, except for the concentration and grain size, which are of a variable nature in each individual sample. In other words, while the traditional approach relies solely on a fitting method, the proposed models autonomously account for the physics of the problem to achieve this. Furthermore, since sample *J* has almost the same particle size distribution as *G*, the same calibration parameters are also used for it with different particle size. This is done intentionally to analyze the efficiency of the extended models in considering the effect of particle size in viscosity modeling.

In particular, the models have an inherent ability to discriminate between different measurements on the basis of their concentration and particle size values. This is a marked departure from the conventional Cross model, which by design does not incorporate concentration as a discriminative factor.

Table 2 provides a detailed compilation of the calibration parameters employed in modeling the viscosity using both proposed models for samples denoted as *G* and *J*. These parameters are crucial in fine-tuning the viscosity models to align with the observed rheological behavior of the respective samples. The calibration process involves adjusting these parameters to optimize the models accuracy. As presented by this table, the same calibration parameters are used for each sample for each model. The only distinguishing parameter is the value of the particle size, which represents an accurate prediction of the viscosity for each sample. However, it should be noted that the two proposed hypotheses represent completely different conceptual frameworks and assumptions, each offering a unique perspective on the matter under investigation. The first hypothesis suggests that as the floc size df increases, the number of flocs *N* also increases, resulting in a decrease in the number of primary particles *P* and consequently a decrease in the rate of change of the linkage dL/dt. On the other hand, the second hypothesis proposes a direct correlation between floc size and the number of links between particles. It is important to recognize that these hypotheses come from different theoretical frameworks, and each offers a unique interpretation of the underlying mechanisms at play. While the calibration parameters for each hypothesis may appear similar, they are derived from fundamentally different perspectives. Therefore, while the calibration parameters may appear identical, they are tailored to reflect the specific nuances and assumptions inherent in each hypothesis. For this reason, Table 2 shows dramatically different calibration values for the same parameters when using the two different models.

The flow curves obtained by Eq. (31) and the measured results of the tested sample $M_{0.100} - M_{0.055}$ are shown in Fig. 15. As can be seen from this figure, an important attribute of sample *M* is that its viscosity increase at low shear rates. This characteristic is absent in samples *G* and *J*. The main objective is therefore to demonstrate that the proposed model can effectively account for this viscosity behavior, unlike the original Cross model which fails to do so. This phenomenon can be explained by the fact that at low shear rates, aggregation dominates the breakup process, resulting in an increase in floc size. This increase in floc size subsequently causes an increase in viscosity. However, once the shear rate exceeds a certain threshold to effectively break up the flocs, a

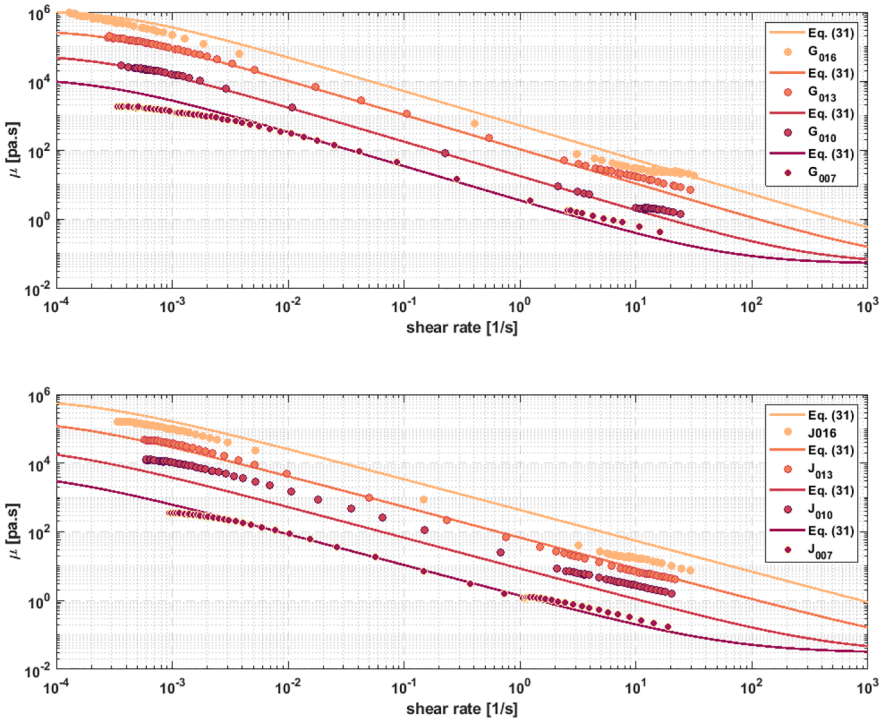

Fig. 13. Gandersum (*G*) and Jemgum (*J*) silt samples with the volumetric solid fractions $\phi_s = 0.16, 0.13, 0.10$ and 0.07, and the flow curves obtained by Eg. (31).

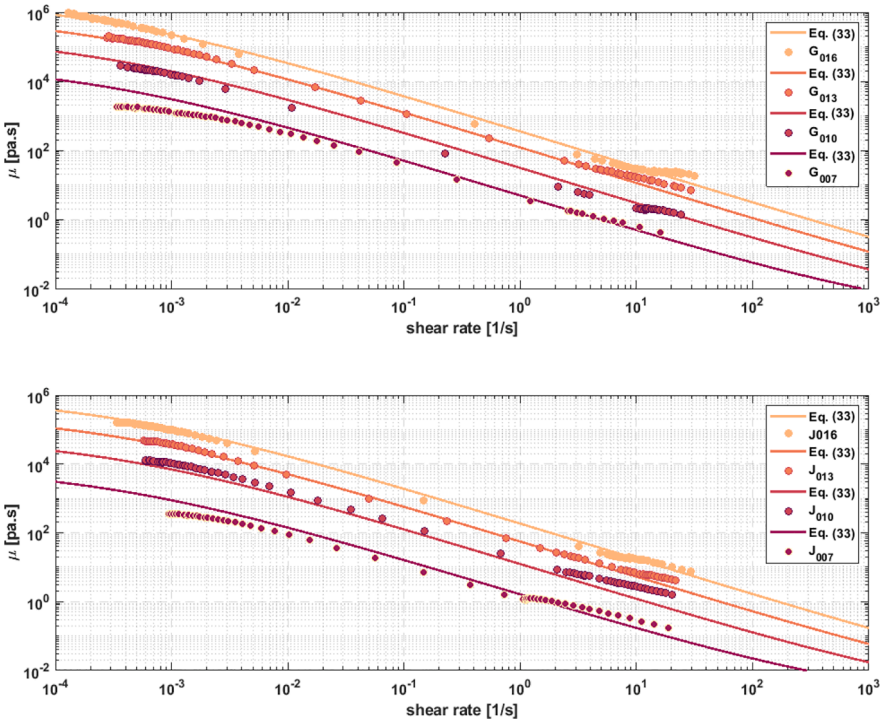

Fig. 14. Gandersum (*G*) and Jemgum (*J*) silt samples with the volumetric solid fractions ϕ_s = 0.16, 0.13, 0.10 and 0.07, and the flow curves obtained by Eg. (33).

Table 2
Calibration parameters used to model the viscosity for samples *G* and *J*.

Model	Sample	Calibration parameters										
		d_p	α'	β	β'	q	n	n_f	k_0'	m	μ_0	μ_∞
Eq. (31)	*G*	15.2e−6	0.07	4e3	1e4	0.11	1.0	1.8	7.6e11	–	6e3	5e−2
	J	17.4e−6	0.07	4e3	1e4	0.11	1.0	1.8	7.6e11	–	6e3	5e−2
Eq. (33)	*G*	15.2e−6	0.5	–	7.0	0.2	–	–	7.6e−7	0.48	–	–
	J	17.4e−6	0.5	–	7.0	0.2	–	–	7.6e−7	0.48	–	–

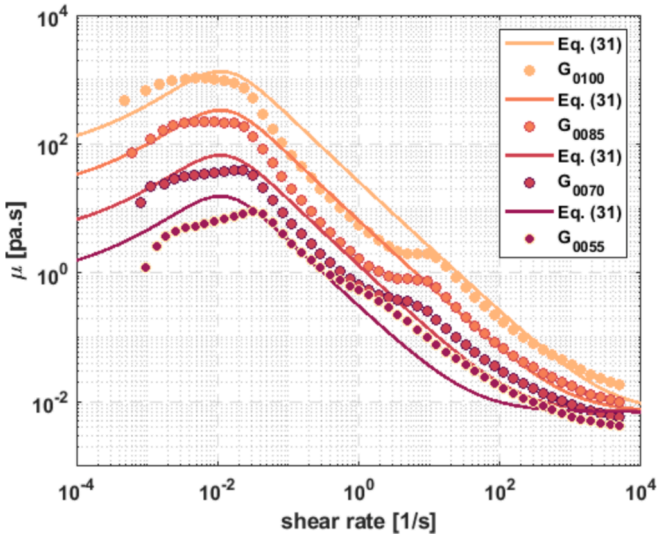

Fig. 15. Silt sample (*M*) with the volumetric solid fractions ϕ_s = 0.100, 0.085, 0.070 and 0.055, and the flow curves obtained by Eq. (31).

decrease in viscosity begins. The results show that the first proposed model is able to model this fact.

Fig. 16 illustrates the results derived from Eq. (33). It is apparent that Eq. (33), due to its simplified nature, does not accurately capture the initial increase in viscosity at low shear rates, unlike the first proposed model which demonstrated this capability. As expected, the viscosity decreases continuously with increasing shear rate. The results also indicate that the second model behaves similarly to the classical Cross model at low shear rates, while additionally incorporating the effect of concentration in values of μ_0. Comparing the results of the first and second proposed models for sample *M*, it is evident that the first model offers superior advantages over the second. From a mathematical perspective, the pre-factor in Eq. (31) increases with the shear rate. However, when the shear rate reaches a critical value, or becomes sufficiently high, the second term (originating from the original Cross model) dominates, leading to a reduction in viscosity as the shear rate continues to increase. This factor not only accounts for the effects of particle diameter and concentration but also demonstrates that very low shear rates can enhance particle adhesion, thereby increasing viscosity. Conversely, Eq. (33) represents a simplified model where viscosity continuously decreases with increasing shear rate, characterized by a single shear rate parameter in the denominator of the equation.

The observed discrepancy in Figs. 13–16 is partly due to the decision not to perform a separate calibration process for each individual sample. Although performing such a calibration could potentially improve the

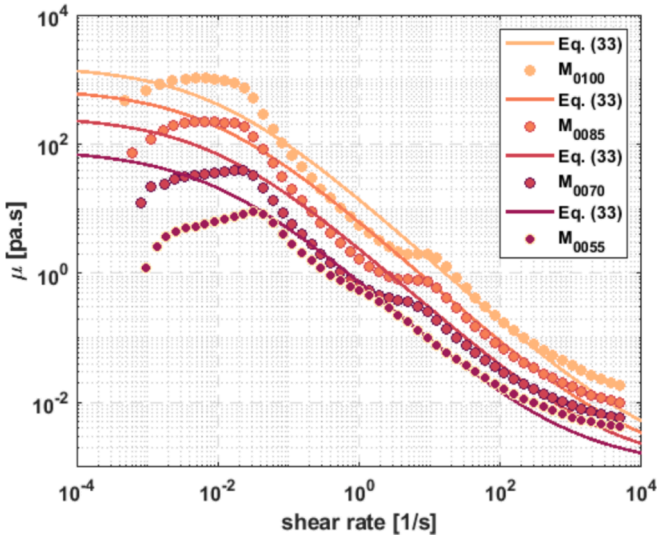

Fig. 16. Silt sample (*M*) with the volumetric solid fractions $\phi_s = 0.100$, 0.085, 0.070 and 0.055, and the flow curves obtained by Eq. (33).

agreement, we deliberately chose not to do so in order to highlight the robustness of our proposed model. Our goal was to demonstrate how effectively the new formulations account for variations in particle size and concentration. It is assumed that the primary differences between samples are in their concentrations and mean sediment sizes. Consequently, an attempt was made to illustrate how the proposed models can accurately respond to these variations in particle size and concentration.

5. Conclusion

This study addresses a significant gap in the existing models used for understanding the non-Newtonian behavior of fluids, particularly in the context of suspensions and colloidal systems. The commonly overlooked factors of particle size, grain size distribution, and concentration are crucial determinants of viscosity and flow behavior in such systems. The proposed mathematical extensions of the Cross flow curve model take a noteworthy step by incorporating these factors explicitly. By considering a variable total number of individual particles in unit volume, these extensions provide a more accurate representation of real-world scenarios where these parameters may vary. The flexibility of the extended model allows for the simulation of a wide range of flow behaviors, including shear-thinning, Newtonian, and shear-thickening, under different shear rates and concentrations.

The model was rigorously tested against measured samples from the Ems estuary, a real-world environment with its own complexities and variations. The results of this validation process showed an acceptable degree of agreement between the model predictions and the empirical data. The successful agreement between model predictions and measured data from the Ems estuary suggests that this extended cross-flow curve model holds promise for accurately capturing the nuances of fluid behavior in complex environments. As a result, it not only contributes to the theoretical understanding of fluid–solid interactions, but also provides a valuable tool for practical applications, particularly in the study and design of suspensions and colloidal systems in natural estuarine environments.

This comprehensive approach contributes valuable insights for the study and design of suspensions, colloidal systems, and complex fluid–solid interactions, enhancing the predictive capabilities of viscosity and flow curve models in practical applications.

The proposed models can be extended by considering a weighted average or an integration over the grain size distribution to account for the contribution of all sediment fractions. Given the nearly identical grain size distributions (GSD) for samples *G* and *J*, and the absence of GSD information for sample *M*, it is advisable to extend this research through additional experiments. Conducting further experiments, and testing the proposed equations for considering the GSD could provide valuable insights into the influence of varying GSD on the rheological properties of these materials.

Declaration of competing interest

The authors declare that they have no known competing financial interests or personal relationships that could have appeared to influence the work reported in this paper.

Data availability

The data supporting the findings of this study are available from the corresponding author upon reasonable request. The data are not publicly available and due to the fact that the data used in the study are owned by a third party, access permissions may be required from the data owner.

Acknowledgements

This work is performed in the framework of the research project ELMOD and was funded by Bundesministerium für Bildung und Forschung (BMBF) and executed by Jülich Forschungszentrum.

References

Ali, W., Chassagne, C., 2022. Comparison between two analytical models to study the flocculation of mineral clay by polyelectrolytes. Cont. Shelf Res. 250, 104864.
Ancey, C., 2001. Role of lubricated contacts in concentrated polydisperse suspensions. J. Rheol. 45 (6), 1421–1439.
Ancey, C., Jorrot, H., 2001. Yield stress for particle suspensions within a clay dispersion. J. Rheol. 45 (2), 297–319.
Carreau, P.J., 1972. Rheological equations from molecular network theories. Trans. Soc. Rheol. 16 (1), 99–127.
Casson, N., 1959. Rheology of disperse systems. Flow Equation for Pigment Oil Suspensions of the Printing Ink Type. Rheol. Disperse Syst. 84–102.
Chmiel, O., Naulin, M., Malcherek, A., 2020. Combining Turbulence and Mud Rheology in a Conceptual 1DV Model–An advanced continuous modeling concept for fluid mud dynamics. Die Küste 89.
Cross, M.M., 1965. Rheology of non-Newtonian fluids: a new flow equation for pseudoplastic systems. J. Colloid Sci. 20 (5), 417–437.
Einstein, A., 1905. Eine neue bestimmung der moleküldimensionen (Doctoral dissertation, ETH Zurich).
Eisma, D., 1986. Flocculation and de-flocculation of suspended matter in estuaries. Netherlands J. Sea Res. 20 (2–3), 183–199.
Engelund, F., Zhaohui, W., 1984. Instability of hyperconcentrated flow. J. Hydraul. Eng. 110 (3), 219–233.
Fusier, J., Goyon, J., Chateau, X., Toussaint, F., 2018. Rheology signature of flocculated silica suspensions. J. Rheol. 62 (3), 753–771.
Gularte, R.C., Kelly, W.E., Nacci, V.A., 1979. Rheological methods for predicting cohesive erosion. In: Proc. 15th Annual Conf. of the Marine Technology Soc., New Orleans, LA, pp. 251–258.
Khelifa, A., Hill, P.S., 2006. Models for effective density and settling velocity of flocs. J. Hydraul. Res. 44 (3), 390–401.
Kranenburg, C., 1994. The fractal structure of cohesive sediment aggregates. Estuar. Coast. Shelf Sci. 39 (5), 451–460.
Kuprenas, R., Tran, D., Strom, K., 2018. A shear-limited flocculation model for dynamically predicting average floc size. J. Geophys. Res.: Oceans 123 (9), 6736–6752.
Lapasin, R., Papo, A., Rajgelj, S., 1983. The phenomenological description of the thixotropic behaviour of fresh cement pastes. Rheol. Acta 22 (4), 410–416.
Moore, F., 1959. The rheology of ceramic slips and bodies. Trans. Brit. Ceram. Soc. 58, 470–494.
Perrin, J., 1910. Brownian Movement and Molecular Reality. Taylor and Francis, p. 93. ISBN: 9780486174723.
Scully, M.E., Friedrichs, C.T., 2007. Sediment pumping by tidal asymmetry in a partially mixed estuary. J. Geophys. Res.: Oceans 112 (C7).
Simha, R., 1949. Effect of concentration on the viscosity of dilute solutions. J. Res. Natl. Bur. Stand 42, 409.
Verney, R., Lafite, R., Brun-Cottan, J.C., 2009. Flocculation potential of estuarine particles: the importance of environmental factors and of the spatial and seasonal variability of suspended particulate matter. Estuar. Coasts 32, 678–693.
Winterwerp, J.C., 1998. A simple model for turbulence induced flocculation of cohesive sediment. J. Hydraul. Res. 36 (3), 309–326.